From Interstellar Clouds to Star-Forming Galaxies: Universal Processes?
Proceedings IAU Symposium No. 315, 2015
P. Jablonka, Ph. André & F. van der Tak, eds.

doi:10.1017/S174392131600733X

Observational studies of the formation and evolution of dense cores

Mario Tafalla

Observatorio Astronómico Nacional (IGN)
Alfonso XII 3, E-28014 Madrid, Spain
email: m.tafalla@oan.es

Abstract. Dense cores are the simplest star-forming sites. They represent the end stage of the fragmentation hierarchy that characterizes molecular clouds, and they likely control the efficiency of star formation via their relatively low numbers. Recent dust continuum observations of entire molecular clouds show that dense cores often lie along large-scale filamentary structures, suggesting that the cores form by some type of fragmentation process in an approximately cylindrical geometry. To understand the formation mechanism of cores, additional kinematic information is needed, and this requires observations in molecular-line tracers of both the dense cores and their surrounding cloud material. Here I present some recent efforts to clarify the kinematic structure of core-forming regions in the nearby Taurus molecular cloud. These new observations show that the filamentary structures seen in clouds are often more complex than suggested by the maps of continuum emission, and that they consist of multiple fiber-like components that have different velocities and sonic internal motions. These components likely arise from turbulent fragmentation of the large-scale flows that generate the filamentary structures. While not all these fiber-like components further fragment to form dense cores, a small group of them does so, likely by gravitational instability. This fragmentation produces characteristic chain-like groups of dense cores that further evolve to form stars.

Keywords. stars: formation, ISM: clouds, ISM: kinematics and dynamics, ISM: molecules

1. Introduction

Star formation is largely a fragmentation process. A typical molecular cloud contains tens of thousands of solar masses of material, and to form stars, it needs to fragment into parcels with typically the mass of our Sun. Understanding star formation therefore requires following the process of cloud fragmentation over multiple spatial scales, and identifying the different structures that appear at each of these scales.

In the hierarchy of cloud fragmentation, dense cores occupy a special place. These objects have typical sizes of $\approx$0.1 pc, and in nearby clouds like Taurus, Perseus, or Ophiuchus, they can be easily identified by their obscuration in optical images, by the emission of specific molecular tracers like NH_3 and N_2H^+, or by their concentrated emission in the millimeter-submillimeter dust continuum (Benson & Myers 1989; di Francesco *et al.* 2007; Bergin & Tafalla 2007)

With typical masses of a few $M_\odot$, dense cores have internal motions that are subsonic, and this indicates that thermal pressure dominates over non-thermal motions as a source of support against gravity. Cores, in addition, often harbor stellar objects at the earliest evolutionary stages (Beichman *et al.* 1986), a sign that the formation of a core represents the final step in the process of cloud fragmentation just prior to gravitational collapse. This close connection between core formation and star formation is further strengthened by the strong similarity between the distribution of core masses and the stellar initial

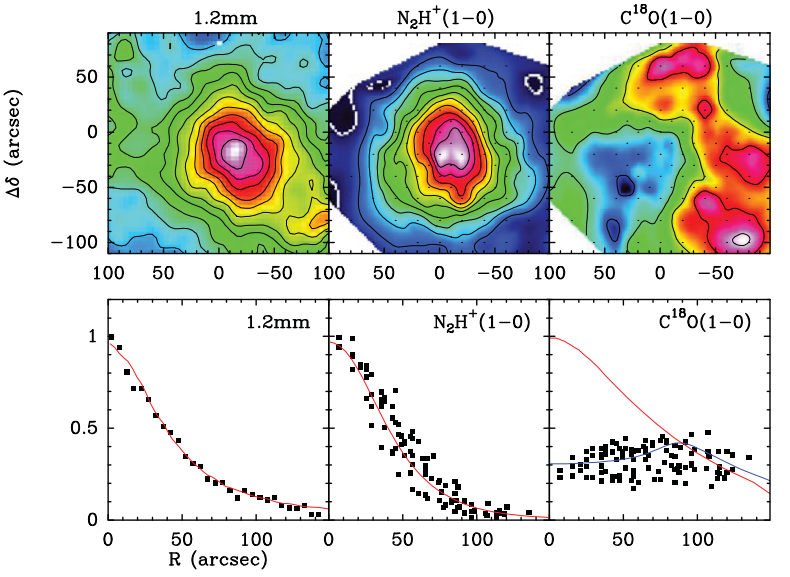

Figure 1. Molecular differentiation in the L1517B core. The top panels show the spatial distribution of three tracers (dust, N_2H^+, and $C^{18}O$), while the bottom panels show their radial profiles assuming spherical symmetry. The dust emission (left) traces the column density of the core, and its radial profile has been used to infer a core density profile. The N_2H^+ emission (middle) shows a similar distribution as the dust emission, and its radial profile is well fitted using a constant abundance law (red line). Finally, the $C^{18}O$ emission (right) seems to avoid the core peak, and the radial profile can only be fitted with a model having a large drop of abundance toward the central part of the core (blue line). Adapted from Tafalla *et al.* (2004). *(A color version of this figure is available online.)*

mass function, which suggests that the mass of the future star is already set at the time of core formation (Motte *et al.* 1998; Alves *et al.* 2007).

2. The need for molecular-line data

Large-scale optical images of clouds have often revealed their strikingly complex and filamentary geometry (Barnard 1907; Schneider & Elmegreen 1979), but only with the arrival of the new dust continuum images from the Herschel Space Observatory has it become clear that a filamentary geometry is a common feature of all clouds, both low and high mass, and both star-forming and quiescent (André *et al.* 2010, Molinari *et al.* 2010). While clouds appear as complex webs of filaments having different sizes and orientations, the dense cores embedded in them tend to be aligned with the filaments like beads along a string, providing a strong impression that the cores must form by some type of fragmentation process that occurs inside the filaments (Arzoumanian *et al.* 2011; André *et al.* 2014; Könyves *et al.* 2015).

Understanding how filaments form and how they later fragment into dense cores and stars requires observations that go beyond the Herschel continuum data. These data, while truly spectacular, are insensitive to the velocity of the gas, so they only provide a limited view of the physical state of the clouds. To complete this view, the Herschel data needs to be combined with observations of molecular line tracers that are sensitive to the internal kinematics of the emitting gas.

Molecular line tracers provide additional information on the state of the gas. For example, the gas chemical composition is sensitive to its evolutionary state, since it

https://doi.org/10.1017/S174392131600733X Published online by Cambridge University Press

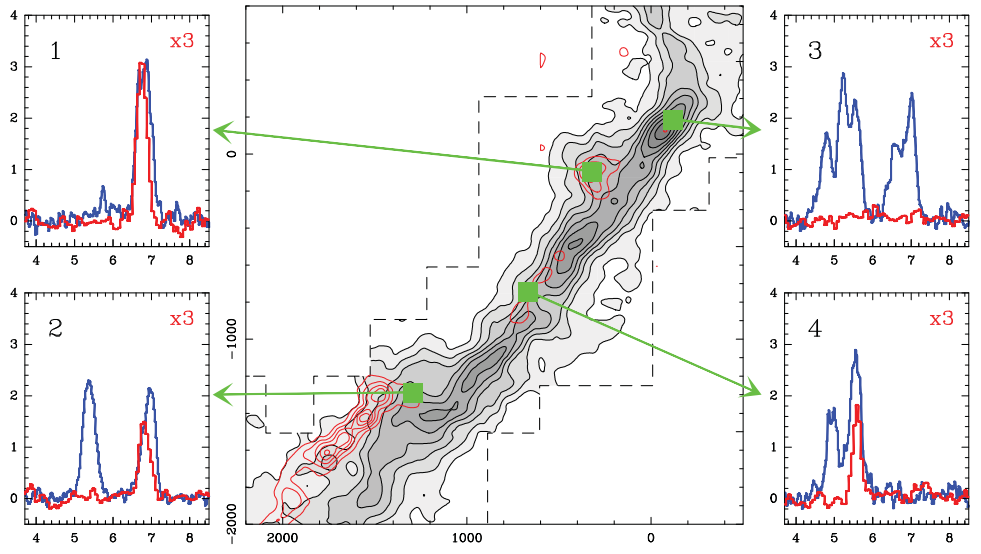

Figure 2. Evidence for multiple velocity components in L1495/B213. The central panel shows a map of $C^{18}O(1–0)$ integrated intensity toward the central part of the cloud. Although the emission appears to arise from a single filamentary region, the spectra at individual positions (left and right panels) reveal the presence of multiple velocity components (blue histograms). These multiple peaks do not arise from self-absorption or similar optical-depth effects, since the isolated $N_2H^+(1–0)$ feature, when detected, coincides with one of the $C^{18}O$ peaks (red histograms). From Hacar *et al.* (2013). *(A color version of this figure is available online.)*

changes significantly during the phase of contraction due to a number of processes, most notably the freeze out molecules onto the cold dust grains (Bergin & Tafalla 2007). This chemical inhomogeneity of the cloud gas can be used to separate its different density regimes by applying a tomographic analysis that combines selected molecular tracers. The densest parts of the cloud (the cores), for example, are chemically evolved and heavily depleted in carbon-bearing molecules like CO, so they are invisible in even the thinnest CO isotopologues, but they are very bright in N-bearing molecules like N_2H^+. The surrounding outer gas, on the other hand, is chemically younger and therefore very weak in N_2H^+, but can easily be traced with CO isotopologues, that in addition of being abundant, have a low-dipole moment that makes them easily thermalized. An example of this technique can be seen in Fig. 1 for L1517B in Taurus, which is a typical representative of a starless core at an intermediate state of evolution.

3. From filaments to fibers

One of the first core-forming regions studied with a combination of N_2H^+ and $C^{18}O$ observations has been L1495/B213 in Taurus (Hacar *et al.* 2013). This region was previously studied in detail using IR extinction and dust continuum observations by Schmalzl *et al.* (2010) and Palmeirim *et al.* (2013), respectively, and appears in the dust images as a single 10 pc-long filament with a number of dense cores and young stellar objects (YSOs) embedded in its interior.

Observations of the L1495/B213 cloud in molecular lines show that the single-filament picture inferred from the dust absorption/emission data is overly simplistic. As Fig. 2 illustrates, even lines of sight where the integrated emission appears as a single filament have $C^{18}O$ spectra with multiple velocity components separated by up to 2 km s^{-1}, which

https://doi.org/10.1017/S174392131600733X Published online by Cambridge University Press

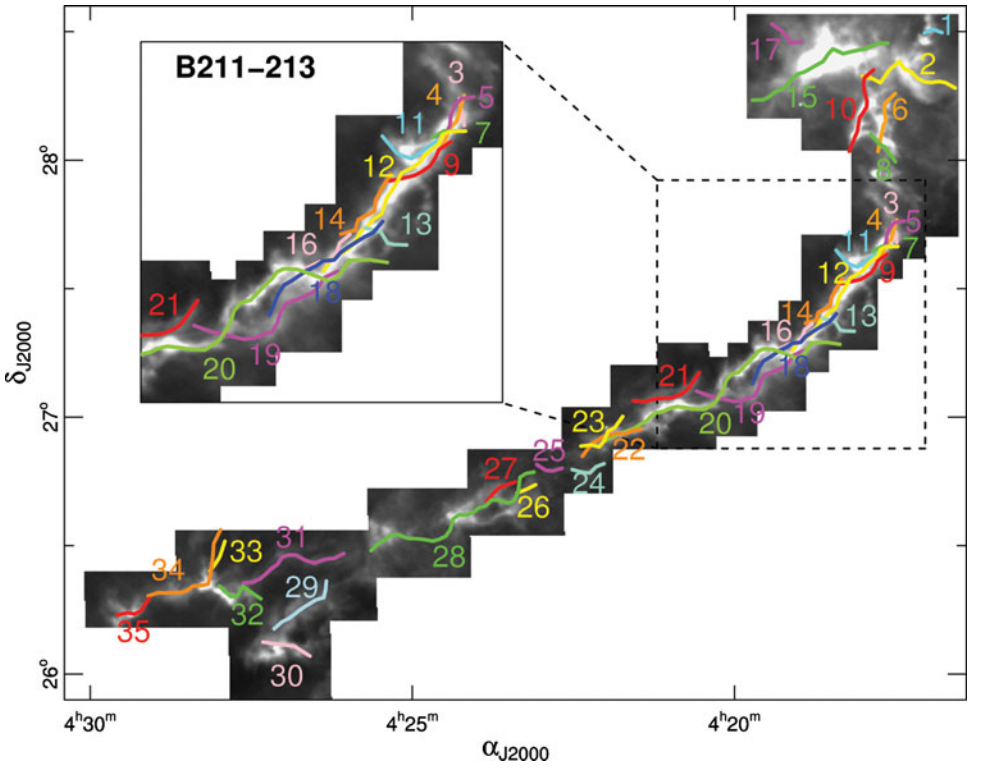

Figure 3. Location of the fibers in L1495/B213. Each colored line represents the central axis of one of the fibers identified from the $C^{18}O$(1–0) emission by Hacar *et al.* (2013). The background grey scale image is the SPIRE 250 μm continuum map from Palmeirim *et al.* (2013). The good agreement between the two components indicates that the dust emission arises from a complex web of velocity-coherent fibers. Figure from Hacar *et al.* (2013). *(A color version of this figure is available online.)*

correspond to a Mach number of 10 for molecular gas at a temperature of 10 K (Hacar *et al.* 2013). This multiplicity of velocity components separated by supersonic speeds already indicates that the fragmentation process by which the L1495/B213 filament has formed its cores must have been far more complex than expected from the dust emission analysis.

To understand the underlying structure of the L1495/B213 region, Hacar *et al.* (2013) disentangled the overlapping velocity components. They first fitted multiple Gaussian profiles to each $C^{18}O$ spectrum, estimating the number of velocity components present at each position, and for each component, deriving its velocity centroid and velocity dispersion. Then, they connected the velocity components at different positions using a friends-of-friends algorithm similar to that used in redshift surveys to identify clusters of galaxies. With this procedure, Hacar *et al.* (2013) found that the $C^{18}O$ emission of the L1495/B213 region can be understood as resulting from 35 velocity components that lie more or less evenly spread along the full length of the "single" filament seen in the dust maps. Fig. 3 shows a representation of these components overlayed on the dust continuum map from Palmeirim *et al.* (2013).

While the velocity components in L1495/B213 have different sizes and masses, they tend to share a number of properties. First of all, they tend to be elongated, and their aspect ratios are typically larger than 4. For this reason, they are often referred to as

https://doi.org/10.1017/S174392131600733X Published online by Cambridge University Press

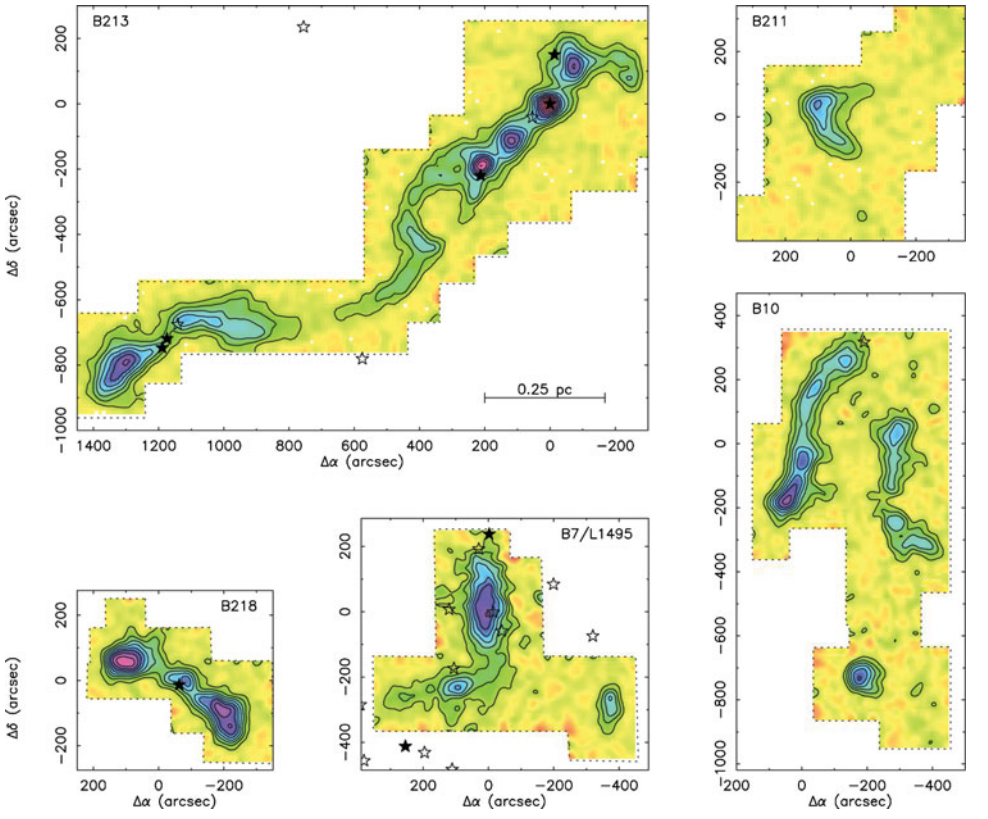

Figure 4. Maps of N_2H^+ (1–0) emission toward the regions with dense cores in L1495/B213. Note how the cores mostly form small linear groups of several compact cores connected by extended emission. These "chains" of cores seem to form from the fragmentation of the $C^{18}O$ fibers. From Tafalla & Hacar (2015).

"fibers," to distinguish them from the large-scale L1495/B213 "filament." The internal velocity field of these fibers presents large-scale oscillations, and the non-thermal component of the linewidth lies near the sonic-transonic boundary. In addition, a number of fibers have mass per unit length ratios of about 16 $M_\odot$ pc^{-1}, which approximately corresponds to the expected value for a cylinder in hydrostatic equilibrium at 10 K (e.g., Stodólkiewicz 1963; Ostriker 1964).

The discovery of multiple fibers in what initially appeared to be a single filament may seem surprising, but a number of recent simulations have shown that fiber-like structures form naturally. Moeckel & Burkert (2015), for example, have presented simulations of a self-gravitating turbulent cloud, and have found multiple fiber-like structures with oscillatory velocity fields similar to those seen in L1495/B213. Other simulations that show evidence for fiber-like structures are those by Kritsuk *et al.* (2013), Smith *et al.* (2016), and Li *et al.* (2015), who have simulated the formation and evolution of turbulent molecular clouds with different masses and sizes. While not all these fiber-like structures may have the same properties as the L1495/B213 fibers, their common sight in simulations suggests that the formation of multiple velocity components in the gas does not require a special tuning in the initial conditions. Understanding in detail how these structures form remains however an important issue.

https://doi.org/10.1017/S174392131600733X Published online by Cambridge University Press

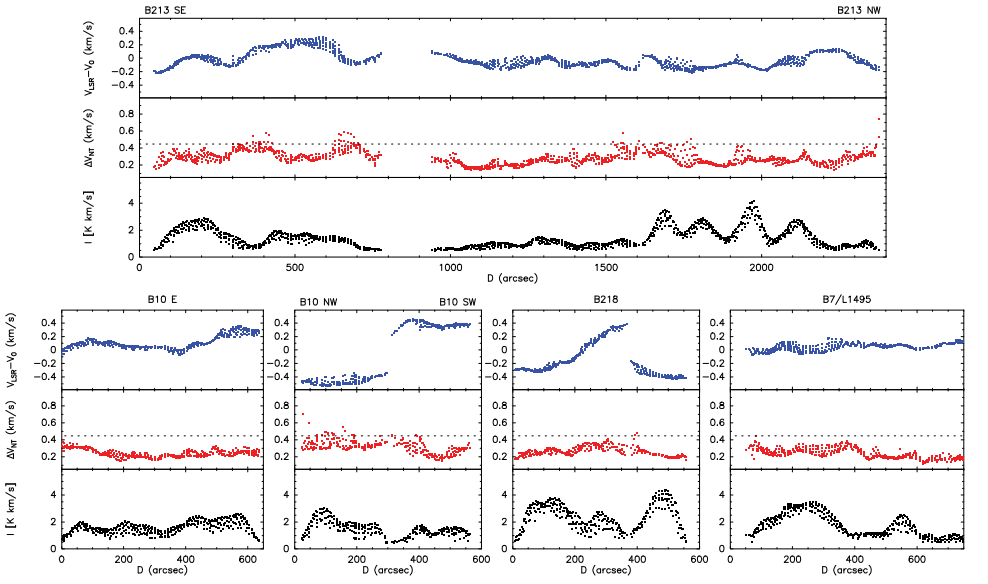

Figure 5. Internal kinematics of the core chains. Central velocity (top, blue symbols), non-thermal linewidth (middle, red symbols), and integrated intensity (bottom, black symbols) of N_2H^+(1–0) along the axis of each chain shown in Fig. 4. Note the large-scale coherence of the velocity and the mostly subsonic internal motions. A few positions with enhanced kinematics seem to be associated with stellar feedback. See Tafalla & Hacar (2015) for further details. *(A color version of this figure is available online.)*

4. From fibers to cores

So far, we have seen the behavior of the $C^{18}O$ emission which, for chemical reasons, traces the low density gas in L1495/B213. To study the population of dense cores in the cloud, we now use N_2H^+, which is immune to depletion at typical core densities and therefore traces the dense gas. Fig. 4 shows N_2H^+(1–0) maps of the dense cores in L1495/B213 obtained with the IRAM 30m telescope by Tafalla & Hacar (2015). As can be seen, most dense cores belong to small linear groups of a few condensations each connected by more extended emission. These core groups, which we will refer to as "chains," seem to be associated with some of the fibers identified in $C^{18}O$, since they coincide with them in both position, orientation, and velocity. Quantitatively, of a total of 19 cores in the L1495/B213 region, 14 ($\approx$70%) are associated with just 4 fibers, while the remaining 5 cores are more of less isolated.

This association of the majority of cores with a small number of fibers suggests that fibers can be classified in two groups. On the one hand, about 28 of the 35 fibers in the cloud (i.e., 80%) are not associated with any dense core, and therefore seem to be sterile. The remaining 20% of the fibers, on the other hand, is responsible for the whole core population, which means that each of these fibers has produced on average almost 3 dense cores. Fibers, therefore, seem to either be sterile and form no cores, or produce a small group of 2 or 3 cores, and in this case we classify them as fertile.

The fertile/sterile dichotomy suggests that some fibers are more prone than others to form dense cores, and therefore, that core formation results from an intrinsic property of the fiber as a whole. The property most likely to separate fertile and sterile fibers is the mass per unit length, although our line data are not ideal to determine masses due to the depletion of CO and the uncertain abundance of N_2H^+. The $C^{18}O$ data of Hacar *et al.* (2013), however, suggest that that core-forming fibers have a slightly higher mass

https://doi.org/10.1017/S174392131600733X Published online by Cambridge University Press

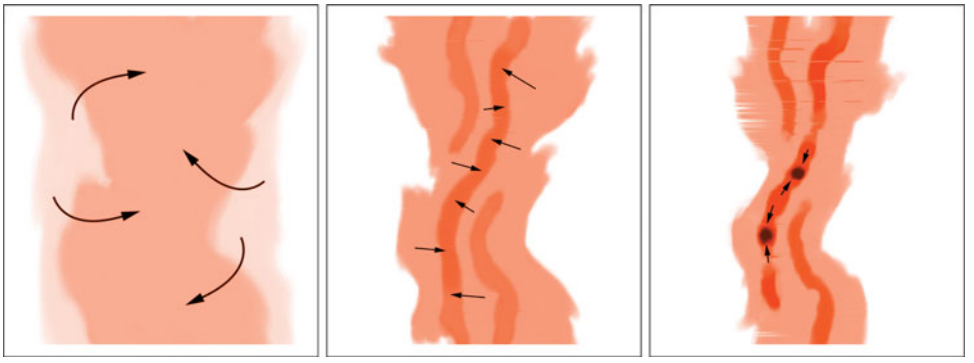

Figure 6. *Fray and fragment* scenario of core formation in L1495/B213 (Tafalla & Hacar 2015).

per unit length than the fibers that do not form cores, and that the fertile fibers lie close to the 16 $M_\odot$ pc^{-1} threshold of gravitational instability predicted by a simple model of a pressure-supported isothermal cylinder at 10 K (Stodólkiewicz 1963; Ostriker 1964).

To further explore the mechanism of core formation in fertile fibers, Fig. 5 presents a series of velocity profiles along each of the core chains. As can be seen, most chains have oscillatory velocity profiles (top panels, blue symbols), with the only exception of B218, where the dense gas seems to be accelerated by the outflow from the central source. The coherent velocity profiles of the chains match those of the larger-scale $C^{18}O$ fibers, indicating that core formation has occurred without a significant change in the gas kinematics.

Further evidence for a quiescent process of core formation comes from the analysis of the non-thermal linewidth profiles (middle panels, red symbols). These profiles show that the overwhelming majority of the points have subsonic internal motions, and that the few points with supersonic linewidths are mostly associated to feedback from the embedded YSOs (see Tafalla & Hacar 2015 for further details). Such quiescent state of the gas over chain scales strongly suggests that core formation has occurred without appreciable changes in the velocity field, or in other words, without the presence of internal shocks. These characteristics are most consistent with a process of gravitational fragmentation that starts in a rather quiescent state.

While the gas in the fibers and cores is extremely quiescent, the process of core formation deviates from that predicted by the theory of exponential growth of infinitesimal perturbations. In this simplest instability mode, all cores are expected to form simultaneously by the non-linear growth of a sinusoidal initial perturbation. As the maps in Fig. 4 show, however, cores with stars alternate with cores without stars in the same chain without displaying a systematic pattern. Chains B213SE and B218, for example, have a YSO at the center and two starless cores at the sides, which is the opposite to what is expected in the case of fragmentation of a truncated cylinder, where star formation should occur at the edges because they are more unstable due to the asymmetry in the gravitational field (Burkert & Hartmann 2004).

If cores with and without stars alternate in the same chain (e.g., B213NW), the formation and evolution of the cores must not occur simultaneously across the chain. Most likely, the fibers form with non-negligible density perturbations imprinted on them, and the growth of these perturbations leads to core formation. To test these ideas, a more systematic effort to study core formation in irregular cylindrical systems is needed.

https://doi.org/10.1017/S174392131600733X Published online by Cambridge University Press

5. A "fray and fragment" scenario of core formation

Our analysis of core formation has focussed on the L1495/B213 region in Taurus, but preliminary work on other regions, together with published results from different clouds (Henshaw *et al.* 2014) and the results from the already-mentioned simulations, suggest that the L1495/B213 results are likely to common. If so, core formation would appear to involve two different physical processes. The first one is the formation of multiple velocity-coherent fibers, which as shown by simulations, likely results from the dissipation of turbulence in shocks between large-scale streams of gas. The second step in the process is the fragmentation of some of the fibers, which is likely driven by gravity in those fibers that have reached the instability threshold of mass per unit length. These two different processes are illustrated schematically in Fig. 6 for a geometry similar to that of L1495/B213. We call this two-step scenario "fray and fragment," with "fray" referring to the production of multiple fibers and "fragment" referring to their gravitational fragmentation. If correct, it suggests that dense cores are, by formation, gravitationally unstable, and that their evolution can only further lead to the formation of stars.

Acknowledgements

It is a pleasure to thank Álvaro Hacar for a fruitful and ongoing collaboration from which many of the results presented here have originated. I also thank the Spanish MINECO for funding support from grants AYA2012-32032 and FIS2012-32096, and the organizers of the meeting for their invitation to present this work.

References

Alves, J., Lombardi, M., & Lada, C. J. 2007, *A&A*, 462, L17
André, P., Men'shchikov, A., Bontemps, S., *et al.* 2010, *A&A*, 518, L102
André, P., Di Francesco, J., Ward-Thompson, D., *et al.* 2014, *Protostars and Planets VI*, 27
Arzoumanian, D., André, P., Didelon, P., *et al.* 2011, *A&A*, 529, L6
Barnard, E. E. 1907, *ApJ*, 25, 218
Beichman, C. A., Myers, P. C., Emerson, J. P., *et al.* 1986, *ApJ*, 307, 337
Benson, P. J. & Myers, P. C. 1989, *ApJS*, 71, 89
Bergin, E. A. & Tafalla, M. 2007, *ARAA*, 45, 339
Burkert, A. & Hartmann, L. 2004, *ApJ*, 616, 288
di Francesco, J., Evans, N. J., II, Caselli, P., *et al.* 2007, *Protostars and Planets V*, 17
Hacar, A., Tafalla, M., Kauffmann, J., & Kovács, A 2013, *A&A*, 554, A55
Henshaw, J. D., Caselli, P., Fontani, F., Jiménez-Serra, I., & Tan, J. C. 2014, *MNRAS*, 440, 2860
Könyves, V., André, P., Men'shchikov, A., *et al.* 2015, *A&A*, 584, A91
Kritsuk, A. G., Lee, C. T., & Norman, M. L. 2013, *MNRAS*, 436, 3247
Li, P. S., McKee, C. F., & Klein, R. I. 2015, *MNRAS*, 452, 2500
Moeckel, N. & Burkert, A. 2015, *ApJ*, 807, 67
Molinari, S., Swinyard, B., Bally, J., *et al.* 2010, *A&A*, 518, L100
Motte, F., André, P., & Neri, R. 1998, *A&A*, 336, 150
Ostriker, J. 1964, *ApJ*, 140, 1056
Palmeirim, P., André, P., Kirk, J., *et al.* 2013, *A&A*, 550, A38
Schmalzl, M., Kainulainen, J., Quanz, S. P., *et al.* 2010, *ApJ*, 725, 1327
Schneider, S. & Elmegreen, B. G. 1979, *ApJS*, 41, 87
Smith, R. J., Glover, S. C. O., Klessen, R. S., & Fuller, G. A. 2016, *MNRAS*, 455, 3640
Stodólkiewicz, J. S. 1963, *AcA*, 13, 30
Tafalla, M., Myers, P. C., Caselli, P., & Walmsley, C. M. 2004, *A&A*, 416, 191
Tafalla, M. & Hacar, A. 2015, *A&A*, 574, A104